IECE Transactions on Intelligent Unmanned Systems
http://dx.doi.org/10.62762/TIUS.2024.557673

RESEARCH ARTICLE

Model Predictive Control for Enhanced Trajectory Tracking of Autonomous Deep-Sea Tracked Mining Vehicles

Hongyun Wu[1], **Yuheng Chen**[2,*] **and Hongmao Qin**[2]

[1] Changsha Institute of Mining Research, Changsha 410000, China
[2] Key Laboratory of Advanced Design and Manufacturing for Vehicle Body, College of Mechanical and Vehicle Engineering, Hunan University, Changsha 410082, China

Abstract

This paper explores the effectiveness of Model Predictive Control (MPC) for trajectory tracking in autonomous deep-sea tracked mining vehicles operating within polymetallic nodule mining environments, considering model uncertainties and external disturbances. Traditional applications of MPC in autonomous vehicle trajectory tracking, which typically rely on kinematic models under minimal external disturbance, often fail when faced with model inaccuracies and external disruptions. To address these challenges, we propose an MPC-based trajectory tracking algorithm that includes a speed correction controller for the drive wheel. This controller, developed through experimental data fitting, aims to mitigate issues such as vehicle body subsidence and track slippage. Tracking accuracy, particularly in curve navigation, is further enhanced through the use of Kalman Filtering (KF) and Adaptive Kalman Filtering (AKF) to counteract external disturbances. Moreover, we introduce an obstacle avoidance strategy utilizing a tri-circular arc trajectory with uniform curvature for path re-planning. This strategy effectively addresses dead zones and physical obstructions encountered during operation. The superiority of our approach compared to conventional Nonlinear MPC (NMPC) is demonstrated through extensive Simulink and Recurdyn co-simulations.

Keywords: Deep-sea tracked mining vehicle, Trajectory tracking, Model predictive control, Kalman filter, Path planning.

Citation
Wu, H., Chen, Y., & Qin, H. (2024). Model Predictive Control for Enhanced Trajectory Tracking of Autonomous Deep-Sea Tracked Mining Vehicles. IECE Transactions on Intelligent Unmanned Systems, 1(1), 31–43.

1 Introduction

In the twenty-first century, the ongoing depletion of land-based mineral resources coupled with the increasing demand for fossil fuels has precipitated an impending energy crisis. Fortunately, the oceans are abundant in mineral resources such as polymetallic nodules, cobalt-rich crusts, and polymetallic sulfides [1, 2]. Currently, the volume of marine resource deposits that have been explored is hundreds of times greater than those on land, highlighting the urgent need for the development of deep-sea mining technologies.

The deep-sea mining system represents an advanced intelligent transport system, as illustrated in Fig. 1. A mining vehicle descends from the surface support system of a mother ship through a hose to the seabed, where it operates autonomously. The surface support system primarily offers an operational platform for the system and manages the deployment and retrieval of the underwater mineral collection and conveying systems. This support system comprises the mother ship, A-frame, steel frame, winch, and positioning

Academic Editor:
Jinchao Chen

Submitted: 18 May 2024
Accepted: 09 July 2024
Published: 21 July 2024

Vol. 1, **No.** 1, 2024.
10.62762/TIUS.2024.557673

***Corresponding author:**
✉ Yuheng Chen
chenyuheng@csu.edu.cn

system, among other components. The concentrator subsystem is responsible for collecting polymetallic nodules from the seabed and crushing them to an appropriate particle size. This subsystem includes the traveling mechanism, mineral collecting mechanism, crushing mechanism, hydraulic system, measurement and control system, navigation system, positioning system, and acoustic imaging system. The underwater conveying system, which consists of the relay station, hose, hard pipe, and slurry pump, transports the crushed ore to the mother ship's silo. The power conveying system, which includes power containers and cables, supplies power to the underwater system.

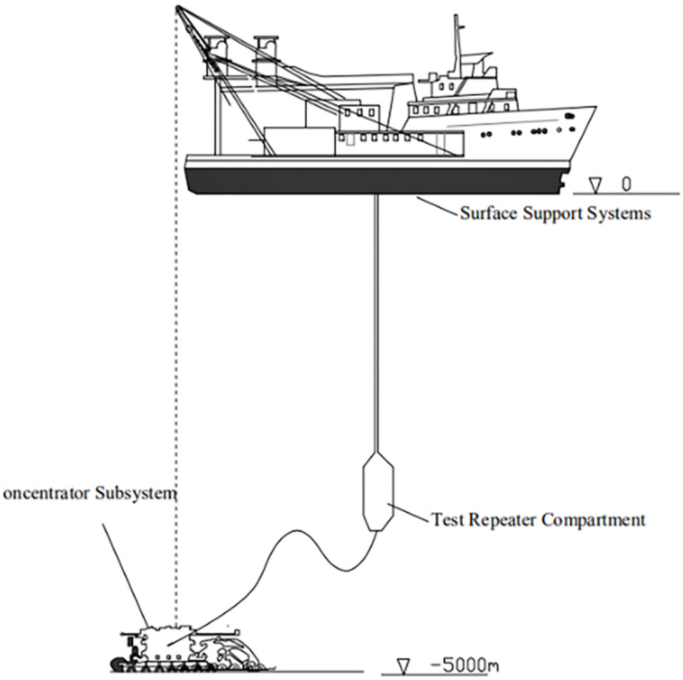

Figure 1. Schematic diagram of the deep-sea mining system.

In the realm of deep-sea mining vehicle dynamics, significant advancements have been made in rigid-body modeling and mechanical analysis. Dai's work utilizing Adams/ATV to simulate mining vehicle dynamics, considering factors such as seabed hydrodynamics and soil shear, has been particularly noteworthy [3]. Concurrently, Liu et al. employed RecurDyn to create rigid-body models of both seabed mining vehicles and surface motherships, conducting co-simulation experiments to examine vehicle dynamics in deep-sea mining systems [4–6].

The unique challenges posed by the soft, thin terrain in polymetallic nodule mining areas necessitate the use of tracked vehicles to mitigate subsidence slip. However, track slippage remains an unavoidable issue that significantly impacts driving performance. This has led to extensive research in trajectory tracking, with Li et al. employing fuzzy PID control to regulate track speeds under various conditions [7–9].

Recent years have seen a shift towards more sophisticated control strategies, particularly model predictive control (MPC), which has found widespread application in autonomous underwater vehicles (AUVs). Researchers have proposed various MPC-based approaches, including adaptive algorithms [10], Lyapunov theory-based controllers [11], and combinations with intelligent algorithms [12, 13]. The integration of nonlinear MPC (NMPC) with sliding mode control has shown particular promise in AUV trajectory tracking [14, 15].

In the automotive sector, MPC has emerged as a powerful tool for trajectory tracking in automated driving systems [16–18]. Hierarchical control strategies, such as those proposed in [19], have been developed to enhance tracking performance. These strategies typically involve multiple steps, including control point selection, trajectory generation, and NMPC implementation. However, challenges remain in ensuring both accuracy and smoothness in trajectory tracking, leading to the development of novel approaches like the quadratic programming method proposed in [21].

Despite its effectiveness, MPC faces challenges related to model mismatches, nonlinearity, and external disturbances. To address these issues, Kalman filtering (KF) techniques have been widely adopted [24], with adaptive Kalman filtering (AKF) showing particular promise in scenarios with model uncertainty [25]. While NMPC methods have demonstrated improved tracking accuracy [26, 27], they often come at the cost of increased computational complexity.

In light of these developments, this paper presents a novel MPC-based trajectory tracking controller for deep-sea tracked mining vehicles. The key contributions of this work are twofold:

1. We introduce an MPC-based algorithm that incorporates a drive wheel speed correction controller to ensure accurate trajectory tracking. This approach accounts for model nonlinearities, vehicle body subsidence, and track slippage. By integrating KF and AKF techniques, the controller effectively manages external disturbances such as ocean currents. Numerical simulations in a simulated soft seabed environment validate

the performance of our approach, demonstrating a balance between control performance and computational efficiency when compared to NMPC methods [28, 29].

2. We propose a trajectory re-planning layer that utilizes an equal-radius tri-circular arc trajectory for obstacle avoidance. This method is particularly suited to tracked vehicles, which have limited yaw angle change capabilities compared to wheeled vehicles. Our approach minimizes frequent yaw angle changes, offering a safer and more efficient obstacle avoidance strategy for deep-sea tracked mining vehicles.

The structure of this paper is as follows: Section 2 outlines the kinematic model of the mining vehicle and the Kalman filter. Section 3 provides a detailed description of the MPC-based trajectory tracking controller and the drive wheel speed correction controller. Section 4 introduces the trajectory re-planning method for complex operating conditions. Section 5 presents and discusses the simulation results, followed by concluding remarks in Section 6.

2 Kinematic Model of the Mining Vehicle

Let ω_1 and ω_2 denote the angular velocities of the left and right track drive wheels, respectively. The coordinates of the vehicle are denoted by (x, y), and ψ represents the yaw angle of the center of mass, as shown in Fig. 2. Thus, we obtain:

$$\begin{cases} v = \frac{v_1+v_2}{2} = \frac{\omega_1+\omega_2}{2} \\ \omega = \frac{v_2-v_1}{2} = \frac{(\omega_2-\omega_1)r}{B} \end{cases} \tag{1}$$

where v is the velocity of the center of mass, ω is the angular velocity, r is the radius of the track drive wheel, and B is the distance between the left and right tracks. The kinematic behavior of the mining vehicle can be described as follows:

$$\begin{bmatrix} \dot{x} \\ y \\ \varphi \end{bmatrix} = \begin{bmatrix} v_x \\ v_y \\ \omega \end{bmatrix} = \begin{bmatrix} \cos\varphi \frac{\omega_1+\omega_2}{2} r \\ \sin\varphi \frac{\omega_1+\omega_2}{2} r \\ \frac{(\omega_2-\omega_1)r}{B} \end{bmatrix} \tag{2}$$

3 Trajectory Tracking Controller Design

Fig. 3 illustrates the components of the mining vehicle's trajectory tracking controller, which comprises an MPC controller, a Kalman filter, and a drive wheel speed correction controller. The MPC controller processes the tracking error information to generate the nominal angular velocities for the left and right track wheels, $\bar{\omega}_1(t+1)$ and $\bar{\omega}_2(t+1)$, respectively. These nominal angular velocities are then fed into the drive wheel speed correction controller, which adjusts them to produce the actual angular velocities $\omega_1(t+1)$ and $\omega_2(t+1)$.

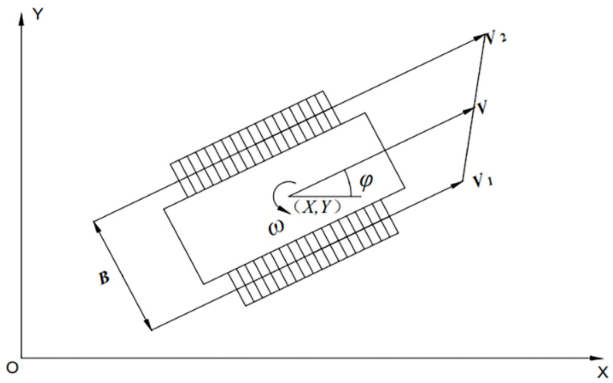

Figure 2. Kinematics model of the mining vehicle.

It is crucial to ensure the stability of both the MPC and the Kalman Filter, as the Kalman Filter mitigates disturbances and noise, while the MPC generates nominal angular velocities. The stability of the proposed trajectory tracking controller is thus guaranteed by the stability of both MPC and KF. The stability proofs for MPC and KF are detailed in [30] and [31], so the stability proof for the proposed controller will not be included in this paper.

3.1 MPC Design

Let N_p and N_c represent the prediction and control horizons, respectively. By applying Euler's method [32], the Jacobian linear approximation of Eq. (2) at each point along the reference trajectory is expressed as:

$$\tilde{X}(t+1 \mid t) = A_t \tilde{X}(t \mid t) + B_t \tilde{U}(t \mid t) \tag{3}$$

where

$$A_t = \begin{bmatrix} 1 & 0 & -\frac{Tr}{2}\left(u_{1ref}(t) + u_{2ref}(t)\right)\sin\varphi_{ref}(t) \\ 0 & 1 & \frac{Tr}{2}\left(u_{1ref}(t) + u_{2ref}(t)\right)\cos\varphi_{ref}(t) \\ 0 & 0 & 1 \end{bmatrix}$$

T is the sampling time.

$$B_t = \begin{bmatrix} \frac{Tr}{2}\cos\varphi_{ref}(t) & \frac{Tr}{2}\cos\varphi_{ref}(t) \\ \frac{Tr}{2}\sin\varphi_{ref}(t) & \frac{Tr}{2}\sin\varphi_{ref}(t) \\ -\frac{r}{B}T & \frac{r}{B}T \end{bmatrix}$$

$$\tilde{X}(t \mid t) = \begin{bmatrix} x_{ref}(t) - x(t) \\ y_{ref}(t) - y(t) \\ \varphi_{ref}(t) - \varphi(t) \end{bmatrix}$$

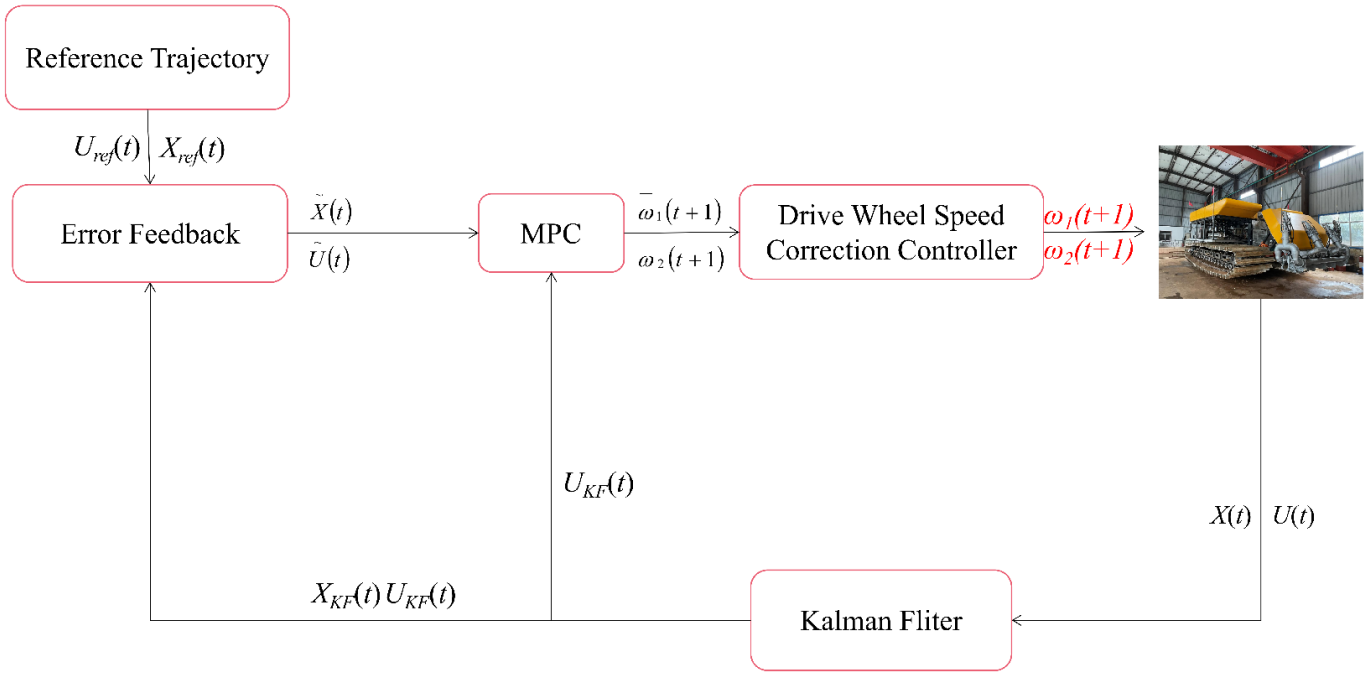

Figure 3. Trajectory tracking control architecture of the mining vehicle.

$$\tilde{U}(t \mid t) = \begin{bmatrix} u_{1ref}(t) - u_1(t) \\ u_{2ref}(t) - u_2(t) \end{bmatrix}$$

Eq. (3) can be further rewritten as [29]:

$$\begin{aligned} \xi(t+1 \mid t) &= \tilde{A}_t \xi(t \mid t) + \tilde{B}_t \Delta u(t \mid t) \\ \eta(t \mid t) &= \tilde{C} \xi(t \mid t) \end{aligned} \tag{4}$$

where

$$\xi(t \mid t) = \begin{bmatrix} \tilde{X}(t \mid t) \\ \tilde{U}(t \mid t) \end{bmatrix}, \tilde{A}_t = \begin{bmatrix} A_t & B_t \\ 0_{2\times 3} & I_3 \end{bmatrix},$$
$$\tilde{B}_t = \begin{bmatrix} B_t \\ I_3 \end{bmatrix}, \tilde{C} = \begin{bmatrix} I_3 \\ 0_{2\times 3} \end{bmatrix}^T.$$

$\Delta u(t \mid t) = [\Delta u_1(t) \quad \Delta u_2(t)]$ is the control input increment.

The predicted output of the system is expressed as follows:

$$Y(t) = \Psi_t \xi(t \mid t) + \Theta_t \Delta U(t) \tag{5}$$

where

$$Y(t) = \begin{bmatrix} \eta(t+1 \mid t) \\ \eta(t+2 \mid t) \\ \cdots \\ \eta(t+N_c \mid t) \\ \cdots \\ \eta(t+N_p \mid t) \end{bmatrix}, \Delta U(t) = \begin{bmatrix} \Delta u(t \mid t) \\ \Delta u(t+1 \mid t) \\ \Delta u(t+2 \mid t) \\ \cdots \\ \Delta u(t+N_c \mid t) \end{bmatrix}$$

$$\Theta_t = \begin{bmatrix} \tilde{C}\tilde{A}_t & 0 & 0 & 0 \\ \tilde{C}\tilde{A}_t\tilde{B}_t & \tilde{C}\tilde{B}_t & 0 & 0 \\ \cdots & \cdots & \ddots & \cdots \\ \tilde{C}\tilde{A}_t^{N_c-1}\tilde{B}_t & \tilde{C}\tilde{A}_t^{N_c-2}\tilde{B}_t & \cdots & \tilde{C}\tilde{B}_t \\ \tilde{C}\tilde{A}_t^{N_c}\tilde{B}_t & \tilde{C}\tilde{A}_t^{N_c-1}\tilde{B}_t & \cdots & \tilde{C}\tilde{A}_t\tilde{B}_t \\ \vdots & \vdots & \ddots & \vdots \\ \tilde{C}\tilde{A}_t^{N_p-1}\tilde{B}_t & \tilde{C}\tilde{A}_t^{N_p-2}\tilde{B}_t & \cdots & \tilde{C}\tilde{A}_t^{N_p-N_c-1}\tilde{B}_t \end{bmatrix}$$

Here we introduced a relaxation factor M to directly restrict control input increments and to guarantee the feasibility. The cost function is shown as follows:

$$J(t) = \sum_{j=1}^{N_p} \|\eta(t+j \mid t)\|_Q^2 + \sum_{j=1}^{N_c-1} \|\Delta u(t+j \mid t)\|_R^2 + \rho M^2 \tag{6}$$

where Q and R are weight-matrices and ρ is a weight coefficient.

Cost function Eq. (6) is transformed into the following form for quadratic programming.

$$J(\xi(t),\Delta U(t)) = \left[\Delta U(t)^T, M\right]^T H_t \left[\Delta U(t)^T, M\right] + G_t \left[\Delta U(t)^T, M\right] \tag{7}$$

where
$H_t = \begin{bmatrix} \Theta_t^T Q \Theta_t + R & 0 \\ 0 & \rho \end{bmatrix}, G_t = [2X(t \mid t) Q \Theta_t, 0].$

The control inputs and their increments are bounded as follows

$$\begin{aligned} \Delta U_{\min} \le \Delta U \le \Delta U_{\max} \\ U\_\min \le D * \Delta U + U \le U\_\max \end{aligned} \tag{8}$$

where $D = \underbrace{\begin{bmatrix} 1 & 0 & \cdots & \cdots & 0 \\ 1 & 1 & 0 & \cdots & 0 \\ 1 & 1 & 1 & \cdots & 0 \\ \vdots & \vdots & \ddots & \ddots & \vdots \\ 1 & 1 & \cdots & 1 & 1 \end{bmatrix}}_{N_c \times N_c} \otimes, \otimes$ is the Kronecker product.

At the current moment t, the optimal control sequence $\Delta U(t)$ is output by addressing the following optimization problem.

$$\begin{aligned} &\min J(\xi(t),\Delta U(t)) \\ &\text{s.t. } \Delta U_{\min} \le \Delta U \le \Delta U_{\max} \\ &U\_\min \le D * \Delta U + U \le U\_\max \end{aligned} \tag{9}$$

The first element $\Delta u(t \mid t)$ of the optimal control sequence $\Delta U(t)$ will be employed as the actual control input increment to generate the input for the drive wheel speed correction controller:

$$\begin{aligned} u_1(t+1) = u_1(t) + \Delta u_1(t) \\ u_2(t+1) = u_2(t) + \Delta u_2(t) \end{aligned} \tag{10}$$

When the mining vehicle operates in a straight line with the heading angle of the preset trajectory set to $0°$, small angle assumptions can be applied to simplify Eq. (2) by eliminating the nonlinear terms $\sin\varphi_{ref}(t)$ and $\cos\varphi_{ref}(t)$. With these assumptions, Eq. (2) can be reformulated as follows:

$$\begin{bmatrix} \dot{x} \\ y \\ \varphi \end{bmatrix} = \begin{bmatrix} v_x \\ v_y \\ \omega \end{bmatrix} = \begin{bmatrix} -\varphi_{ref} \frac{u_{2ref}(t)+u_{1ref}(t)}{2} r \\ \frac{u_{2ref}(t)+u_{1ref}(t)}{2} r \\ \frac{u_{2ref}(t)-u_{1ref}(t)}{B} r \end{bmatrix} \tag{11}$$

and A_t and B_t in Eq. (3) can be rewritten as follows:

$$A_t = \begin{bmatrix} 1 & 0 & -\frac{Tr}{2}\varphi_{ref}\left(u_{1ref}(t)+u_{2ref}(t)\right) \\ 0 & 1 & \frac{Tr}{2}\left(u_{1ref}(t)+u_{2ref}(t)\right) \\ 0 & 0 & 1 \end{bmatrix}$$

$$B_t = \begin{bmatrix} \frac{Tr}{2} & \frac{Tr}{2} \\ \frac{Tr}{2}\varphi_{ref}(t) & \frac{Tr}{2}\varphi_{ref}(t) \\ -\frac{r}{B}T & \frac{r}{B}T \end{bmatrix} \tag{12}$$

3.2 Kalman Filter Design

Discrete model Eq. (1):

$$\begin{cases} X(i+1) = AX(i) + BU(i) + W(i) \\ Y(i) = CX(i) + V(i) \end{cases} \tag{13}$$

where the matrices A and B, the state vector X, and the control input U are consistent with Eq. (3). The matrix C represents the state observation matrix. The vectors W and $V \in \mathbb{R}^3$ denote uncorrelated process noise and observation noise, respectively, with covariance matrices Q and $R \in \mathbb{R}^3$.

The filtering process is as follows:

Prediction of the state:

$$\hat{X}(i+1 \mid i) = A\hat{X}(i \mid i) + BU(i \mid i) \tag{14}$$

Prediction of the covariance matrix:

$$P(i+1 \mid i) = AP(i \mid i)A^T + \Gamma Q \Gamma^T \tag{15}$$

Filter gain matrix updates:

$$K(i+1) = P(i+1 \mid i)C^T \left[CP(i+1 \mid i)C^T + R\right]^{-1} \tag{16}$$

Estimation updates:

$$\begin{cases} X(i+1|i|i) = AX(i \mid i) + K(i+1)\varepsilon(i+1) \\ \varepsilon(i+1) = Y(i+1) - H\hat{X}(i+1 \mid i) \end{cases} \tag{17}$$

Covariance updates:

$$P(i+1 \mid i+1) = \left[I_n - K(i+1)C\right] P(i+1 \mid i) \tag{18}$$

Addressing model uncertainty caused by vehicle body subsidence, track slippage, and measurement noise involves introducing an Adaptive Kalman Filter (AKF). The AKF is selected for its improved capability to provide accurate state estimation despite model nonlinearities [25]. The update parameter d_k is defined as follows:

$$d_k = \frac{1-b}{1-b^k} \tag{19}$$

where b is the forgetting factor constant, with a value ranging between 0.95 and 0.99. Using the update

parameter, the updates for the filter gain matrix in Eq. (16) can be rewritten as follows:

$$\begin{aligned} R(i+1) =& (1-d_{i+1})\,R(i) + CP(i+1\mid i)C^T + \\ & \left(d_{i+1}[I-CK(i)]\varepsilon(i+1)\varepsilon(i+1)^T\right) \\ & [I-CK(i)]^T \\ K(i+1) =& C^T\left[CP(i+1\mid i)C^T + R(i+1)\right]^{-1} \\ & P(i+1\mid i) \end{aligned} \tag{20}$$

The Kalman Filter (KF) is subsequently modified into an Adaptive Kalman Filter (AKF). By introducing the parameter d_k, the impact of accumulated noise from previous time steps is reduced, thereby increasing the weight of current measurements and enhancing robustness against model uncertainties.

3.3 Drive Wheel Speed Correction Controller Design

Track slippage, instantaneous changes in the steering center, and body sinking due to shear forces in polymetallic nodule mines all significantly influence the mining vehicle's performance. To account for these factors, a drive wheel speed correction controller is designed. This controller estimates the complex nonlinear relationship between the angular velocities of the left and right track wheels, ω_{track}, and the actual track travel speed, v_{real}.

Considering these influencing factors, define the track slippage

$$i_i = \frac{v_{real} - v_{ref}}{v_{real}} \tag{21}$$

where v_{ref} and v_{real} represent the theoretical and actual speeds of the track, respectively. Establishing a precise mathematical model for the other two factors is challenging. Thus, the design of the wheel speed correction controller is considered under the concept of incomplete identifiability.

Assuming the maximum driving speed of the mining vehicle is 1.5 m/s, there exists a functional relationship $v_{real} = f(\omega_{track})$ between ω_{track} and v_{real}. To identify this function, a chassis test of the mining vehicle is conducted in a laboratory environment, as illustrated in Fig. 4. In this test, a total of $m = 8$ sets of drive wheel speeds are input into the mining vehicle, and the corresponding actual track speeds are recorded. The function $v_{real} = f(\omega_{track})$ is then obtained by polynomial fitting as follows:

$$\arg\min \sum_{i}^{m} \left(f(\omega_{track}(i)) - v_{real}(i)\right)^2 \tag{22}$$

where $f(\omega_i)$ and $v_{real}(i)$ represent the i-th set of experimental data among the m sets of data. The resulting function is $f = 0.001\left(-2.571x^4 + 48x^3 + 165x^2 + 1858x + 41\right)$, and the fitting result for one track is shown in Fig. 5.

Figure 4. Chassis test in the laboratory environment.

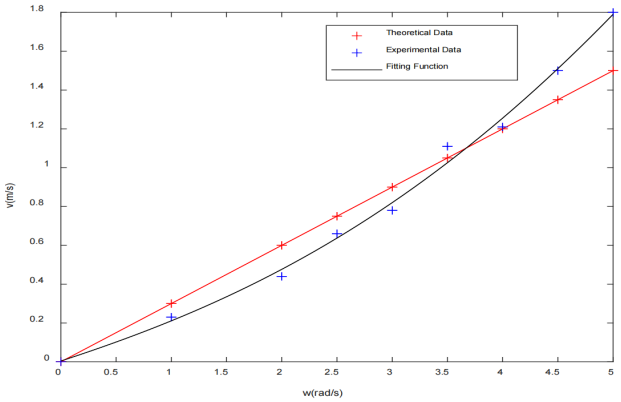

Figure 5. Experimental data fit results.

As illustrated in Fig. 3, the MPC controller generates the desired angular velocities $u_1(t+1)$ and $u_2(t+1)$ for the drive wheels. Using the previously described kinematic model, the desired speeds v_1 and v_2 for the left and right tracks are then determined. Finally, the drive wheel speed correction controller calculates the actual angular velocities as $\omega_1(t+1) = f^{-1}(v_1)$ and $\omega_2(t+1) = f^{-1}(v_2)$.

4 Trajectory Re-Planning in Complex Conditions

The seafloor of the polymetallic nodule mining site is soft, sparse, and relatively flat. In seafloor modeling, slopes of 10° or less are deemed passable, while slopes greater than 10° are considered obstacles. When the mining vehicle encounters a dead zone with impassable slopes on three sides of its pre-set trajectory, it must re-plan its route to back out of the area and

navigate around the obstacles. This section details the trajectory re-planning strategy for the mining vehicle in such scenarios.

4.1 Trajectory Re-Planning for Obstacle Avoidance

The obstacle avoidance trajectory generated should ensure the mining vehicle avoids collisions with obstacles while minimizing deviation from the predetermined path. In recent years, Bessel curves and quintuple polynomial fits [25, 26] have been widely used for obstacle avoidance. These methods typically require frequent adjustments to yaw angles and trajectory curvature within the control algorithm. For four-wheeled vehicles, control inputs are the rear axle speed and steering angle, which allow for frequent changes in yaw angles and trajectory curvature by adjusting the steering angles and rear axle speed.

However, for tracked vehicles, the control inputs are the angular velocities of the left and right track drive wheels, as shown in Eq. (2), which cannot directly alter heading angles and trajectory curvature. The instantaneous curvature ρ of the mining vehicle is given as follows:

$$\rho = \frac{1}{R} = \frac{\omega}{v} = \frac{2\left(\omega_2 - \omega_1\right)}{B\left(\omega_2 + \omega_1\right)} \tag{23}$$

where R is the instantaneous turning radius.

Therefore, the angular velocities of the left and right track drive wheels, ω_1 and ω_2, must be adjusted when the trajectory curvature ρ changes. As previously analyzed, ω_1 and ω_2 require online correction by the drive wheel speed correction controller to mitigate the impact of model uncertainty caused by track slippage and instantaneous changes in the steering center. It is important to note that while the drive wheel speed correction controller can reduce track deviation, it cannot completely eliminate it. In this context, the deviation δ caused by model uncertainty can be expressed as follows:

$$\delta = \begin{bmatrix} \delta_x \\ \delta_y \end{bmatrix} = \begin{bmatrix} \sum_{i=1}^{n} \int_{t_i}^{t_{i+1}} \left(\frac{\Delta\omega_1(i)+\Delta\omega_2(i)}{2}\right) r\cos\varphi(i)dt \\ \sum_{i=1}^{n} \int_{t_i}^{t_{i+1}} \left(\frac{\Delta\omega_1(i)+\Delta\omega_2(i)}{2}\right) r\sin\varphi(i)dt \end{bmatrix} \tag{24}$$

where n is the number of times the angular velocities of the left and right track drive wheels change, and $\Delta\omega_1$ and $\Delta\omega_2$ are the deviations from the desired speed after being processed by the drive wheel speed correction controller.

If the re-planned obstacle avoidance trajectory involves variable curvatures, the complexity of the control algorithm and the trajectory deviation will increase. Therefore, it is essential to minimize curvature changes in the re-planned obstacle avoidance trajectory. Consequently, Bessel curves or quintuple polynomial fits, which require real-time changes in curvature for obstacle avoidance, are unsuitable for the mining vehicle.

In this study, slopes that the mining vehicle cannot cross are considered obstacles. The slope projection forms an irregular approximate circle. To simplify the obstacle model, the geometric center of the slope projection O is chosen as the center of the approximate circle, and the farthest distance from the center to the boundary of the projection is denoted by R, as illustrated in Fig. 6.

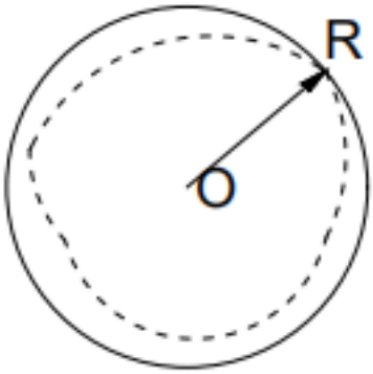

Figure 6. Slope projection.

From Eq. (24), it is evident that the deviation can be minimized by reducing the frequency of changes in the angular velocities of the left and right track drive wheels, denoted as n. Based on this analysis, this study proposes a tri-circular arc obstacle avoidance trajectory with a constant curvature, as shown in Fig. 7. According to Eq. (22), when the mining vehicle travels along a curve with a constant radius, the angular velocities of the left and right track drive wheels remain unchanged. As a result, the deviation of the obstacle avoidance trajectory can be reduced.

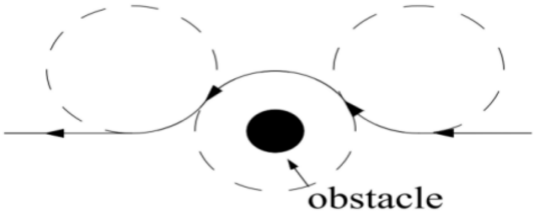

Figure 7. Tri-circular arc avoidance trajectory.

4.2 Trajectory Re-Planning for Dead Zone Escape

When the mining vehicle encounters a dead zone with impassable slopes on three sides of a preset trajectory, operational efficiency is compromised because the vehicle must back out. To address this issue, this study treats the entire dead zone as an obstacle, as illustrated in Fig. 8. By doing so, the mining vehicle can use the previously designed obstacle avoidance method to escape the dead zone.

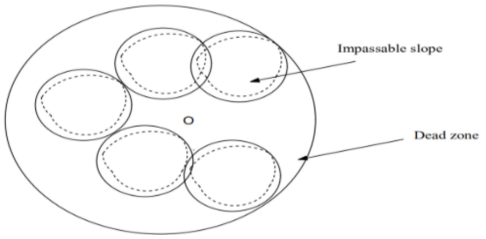

Figure 8. Dead zone.

5 Simulation Verification

This section demonstrates the validation of the proposed MPC tracking algorithm through a co-simulation using RecurDyn and Simulink. The mechanical model of the mining vehicle, as shown in Fig. 9, is constructed in RecurDyn. The parameters of the model are calibrated based on the actual mining vehicle, with details provided in Table 1. The collection route of the mining vehicle is depicted in Fig. 10.

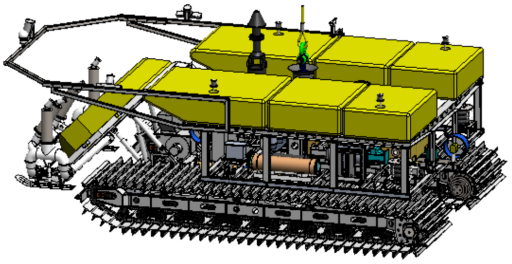

Figure 9. Mechanical model of the mining vehicle.

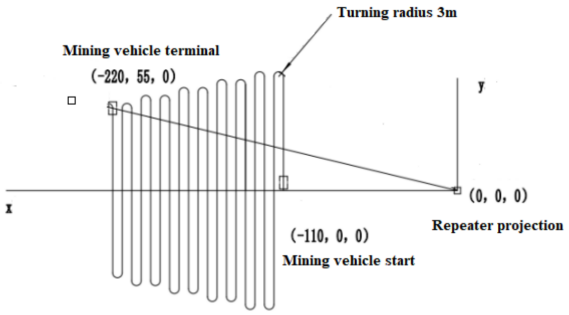

Figure 10. Collection route for the polymetallic nodule mining vehicle.

Table 1. Design parameters for the mining vehicle.

Design Parameter	Value
Land Weight(t)	31
Underwater Weight(t)	11
Length(mm)	8800
Width(mm)	4800
Height(mm)	2950
Drive Wheel Radius(mm)	300
Maximum travel speed(m/s)	1.5
Land Weight(t)	31

During the RecurDyn modeling process, track surface contact parameters, such as the soil shear resistance angle, are configured to simulate the terrain of the polymetallic nodule mining area, as illustrated in Fig. 11.

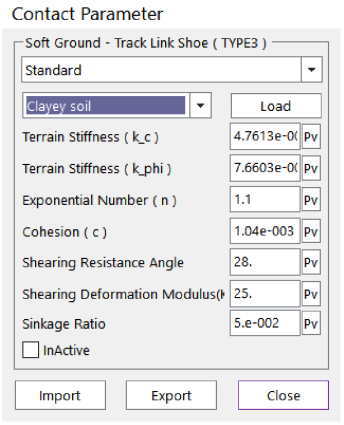

Figure 11. Track contact surface parameters.

5.1 Validation of the Drive Wheel Speed Correction Controller

In this subsection, we validate the effectiveness of the proposed drive wheel speed correction controller. We compare the performance of MPC with and without the proposed drive wheel speed correction controller, and the results are presented in Fig. 12.

As shown in Fig. 12, when the drive wheel speed correction controller is not used, the lateral error starts to increase as the mining vehicle begins to track the first circular trajectory. Simultaneously, the longitudinal position deviates from the reference position. As the vehicle continues to track the second circular trajectory, the lateral error further increases due to instantaneous changes in the steering center, track slippage, and body sinking. This exacerbates the mismatch in the longitudinal position, eventually leading to a failure in trajectory tracking. Conversely, with the drive wheel

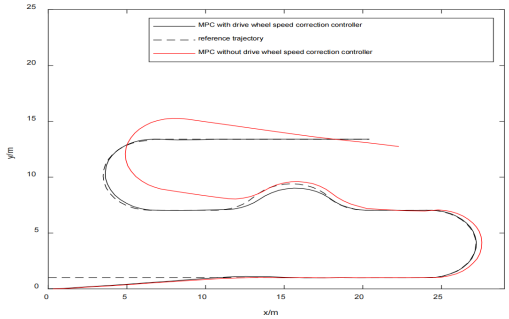

Figure 12. Comparison of MPC with or without the drive wheel speed controller.

speed correction controller in place, the mining vehicle can precisely follow the preset trajectory, thereby demonstrating the controller's effectiveness.

5.2 Validation of the MPC Trajectory Tracking Controller

This subsection evaluates the performance of the MPC-based trajectory tracking controller in two scenarios: with and without obstacles in the preset trajectory.

The reference travel speed is set at 1 m/s. Reference trajectories are generated from 100 discrete sampling points, with a sampling period T of 1 second. To verify the tracking performance of the proposed controller, comparisons are made among MPC, MPC with KF, and MPC with AKF. NMPC is also used in comparative simulation experiments. The deviation, which should not exceed 0.6 meters, is selected as the performance index in the test. Additionally, the trajectory tracking computation times for 100 control cycle loops are recorded during the simulation.

Case 1: Trajectory tracking without obstacles in the preset trajectory

The simulation results for Case 1 are presented in Fig. 13, Fig. 14, and Table 2.

Table 2. MPC trajectory tracking performance evaluation index.

Tracking control	Total computing time	Squared deviation (m)
MPC	313	0.184
MPC with KF	338	0.159
MPC with AKF	345	0.161
NMPC	574	0.141

Fig. 13 illustrates that while NMPC can track straight lines more quickly, MPC, MPC with KF, and MPC with AKF are all effective in tracking the preset linear trajectory. As depicted, these controllers achieve optimal linear tracking performance with minimal deviations.

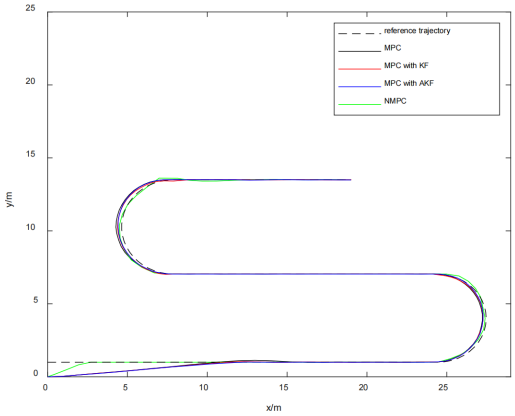

Figure 13. Comparison of vehicle trajectories in the absence of obstacles.

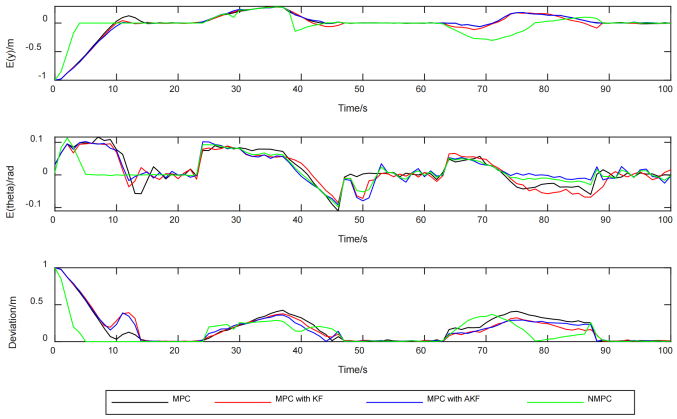

Figure 14. Comparison of tracking deviations in the absence of obstacles.

In Fig. 14, it is evident that without a filter, the MPC tracking controller's trajectory significantly deviates from the preset path during curve tracking. Specifically, the maximum lateral deviation during curve tracking is approximately 0.35 m, and the maximum overall deviation is about 0.42 m, primarily due to lateral deviation.

Further analysis in Fig. 14 shows that with KF, the maximum deviation reduces to around 0.35 m, and the maximum lateral deviation decreases to about 0.25 m. Additionally, with AKF, the maximum deviation is around 0.3 m, with the maximum lateral deviation also at about 0.25 m. Both configurations meet the required tracking performance, indicating that introducing a filter enhances curve tracking by reducing lateral deviation.

Table 2 indicates that the total deviation of MPC with AKF is slightly less than that of MPC with KF, although the computation time for AKF is about 7 seconds longer. Thus, MPC with AKF offers marginally better tracking performance compared to MPC with KF, despite the increased computation time. While NMPC shows superior tracking accuracy, especially in curve tracking, its computation time is significantly longer—approximately 284 seconds more than MPC—resulting in poor real-time performance.

Case 2: Trajectory tracking with obstacles in the preset trajectory

The simulation results for Case 2 are presented in Fig. 15, Fig. 16, and Table 3.

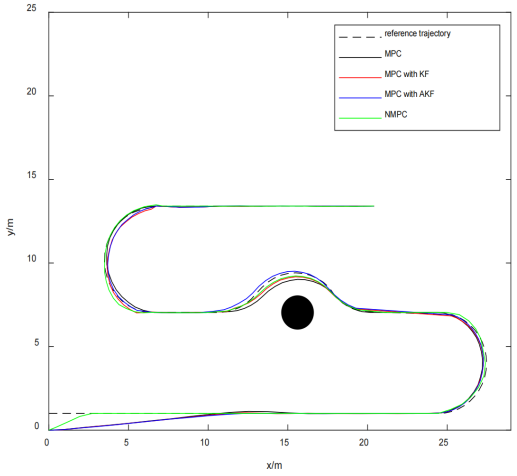

Figure 15. Comparison of vehicle trajectories in the presence of obstacles.

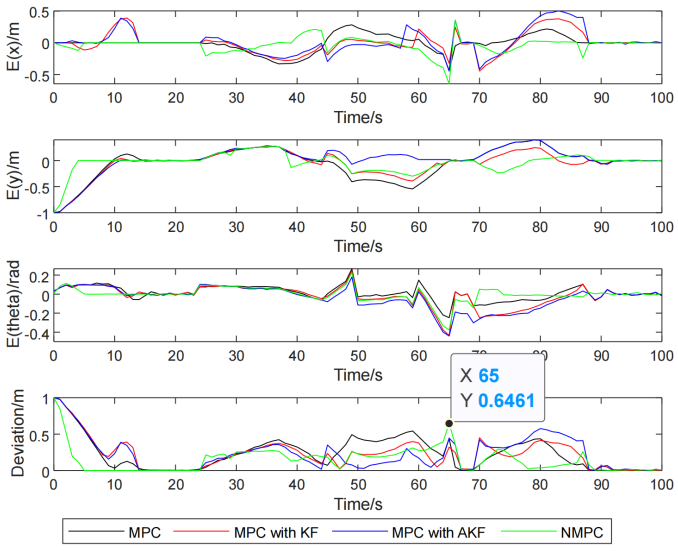

Figure 16. Comparison of tracking deviations in the presence of obstacles.

Table 3. MPC trajectory tracking performance evaluation index.

Tracking control	Total computing time	Squared deviation (m)
MPC	407	0.221
MPC with KF	416	0.190
MPC with AKF	467	0.191
NMPC	683	0.159

Fig. 15 and Fig. 16 demonstrate that MPC, MPC with KF, and MPC with AKF show comparable linear tracking performance.

As seen in Fig. 15, MPC with AKF's trajectory aligns more closely with the reference trajectory during the initial curve tracking, indicating slightly better performance than MPC and MPC with KF.

However, post-obstacle avoidance trajectories of MPC with KF and MPC with AKF exhibit greater deviation compared to MPC alone, as depicted in Fig. 15 and Fig. 16. The second curve tracking performance of MPC with AKF and MPC with KF is marginally inferior to that of MPC.

KF and AKF, based on Markov chain principles [33], imply that each state's moment is influenced by its previous state. This analysis shows that even with limited angular velocity changes, the vehicle encounters model errors from nonlinear terms in Eq. (2), impacting filter estimation accuracy. Introducing AKF or KF leads to incremental model error accumulation during curve tracking. However, small angle assumptions in line tracking, as in Eq. (11), help reduce accumulated errors by eliminating nonlinear terms. Conversely, without AKF or KF, current moment errors more significantly affect each state's moment.

Given the short distance (about 5m) from obstacle avoidance to straight-line tracking to curve tracking, accumulated errors in curve tracking might not be fully addressed within this span. Thus, longer trajectories are necessary to eliminate accumulated errors when using KF or AKF after continuous curve tracking.

Table 3 shows that both MPC with AKF and MPC with KF improve trajectory performance over MPC alone, though not matching NMPC's higher accuracy across the trajectory. MPC with AKF and MPC with KF still meet the accuracy requirements for full trajectory tracking. Notably, NMPC's deviation of 0.6469m, as seen in Fig. 16, fails to meet

accuracy requirements, with NMPC's computation time significantly longer—216 seconds more than MPC. Considering real-time operation needs, NMPC is unsuitable for trajectory tracking.

When avoiding obstacles, the mining vehicle must steer clear of collisions. Fig. 16 and Table 3 reveal that MPC with AKF achieves a smaller maximum lateral deviation than NMPC in obstacle avoidance. Moreover, Fig. 15 shows only MPC with AKF's trajectory does not deviate towards obstacles. Although MPC with AKF's computation time is 50 seconds longer than MPC with KF, it remains acceptable compared to NMPC. Thus, MPC with AKF provides the best obstacle avoidance tracking performance.

6 Conclusion

This study proposes an MPC-based trajectory tracking controller specifically for a mining vehicle. To address the challenges of slippage and model nonlinearity, a drive wheel speed correction controller has been incorporated. Additionally, the Kalman Filter (KF) and Adaptive Kalman Filter (AKF) are utilized to enhance the accuracy of curve trajectory tracking. Numerical simulation results indicate that although MPC with AKF is slightly less accurate than NMPC, it still meets the accuracy requirements while significantly reducing computation time. Furthermore, in the presence of obstacles, MPC with AKF exhibits superior tracking accuracy compared to NMPC.

Conflicts of Interest

The authors declare that they have no conflicts of interest.

Acknowledgement

This work was supported without any funding.

References

[1] Lesage, M., Juliani, C., & Ellefmo, S. L. (2018). Economic block model development for mining seafloor massive sulfides. *Minerals*, 8(10), 468. [CrossRef]

[2] Volkmann, S. E., Kuhn, T., & Lehnen, F. (2018). A comprehensive approach for a techno-economic assessment of nodule mining in the deep sea. *Mineral economics*, 31, 319-336. [CrossRef]

[3] Dai Y, Liu S. An integrated dynamic model of ocean mining system and fast simulation of its longitudinal reciprocating motion[J]. *China Ocean Engineering*, 2013, 27(2): 231-244.[CrossRef]

[4] Dai Y, Liu S. Theoretical design and dynamic simulation of new mining paths of tracked miner on deep seafloor[J]. *Journal of Central South University*, 2013, 20(4): 918-923.[CrossRef]

[5] Dai, Y., Liu, S., & Li, L.(2010). Dynamic analysis of the seafloor pilot miner based on single-body vehicle model and discretized track-terrain interaction model. *China ocean engineering*, 24(1), 145-160.

[6] Li, J., Liu, S., & Dai, Y. (2017). Effect of grouser height on tractive performance of tracked mining vehicle. *Journal of the Brazilian Society of Mechanical Sciences and Engineering*, 39, 2459-2466. [CrossRef]

[7] Dai, Y., & Liu, S. J. (2013). Theoretical design and dynamic simulation of new mining paths of tracked miner on deep seafloor. *Journal of Central South University*, 20(4), 918-923.[CrossRef]

[8] Li, L., Zheng, Z., & Chen, M. (2014) Point stabilization of seabed mining vehicle based on Lyapunov theory, *Journal of Central South University*, vol. 45, no. 08, pp. 2624-2628, 2014.

[9] Li, L., & Zou, Y. H. (2012). Tracking moving path of seabed mining vehicle based on theory of variable universe fuzzy control. *Journal of Central South University*, 43(02), 489-496.

[10] Gan, W., Zhu, D., Hu, Z., Shi, X., Yang, L., & Chen, Y. (2019). Model predictive adaptive constraint tracking control for underwater vehicles. *IEEE Transactions on Industrial Electronics*, 67(9), 7829-7840. [CrossRef]

[11] Shen, C., Shi, Y., & Buckham, B. (2017). Trajectory tracking control of an autonomous underwater vehicle using Lyapunov-based model predictive control. *IEEE Transactions on Industrial Electronics*, 65(7), 5796-5805. [CrossRef]

[12] Chen, Y., Xie, X., Zhang, T., Bai, J., & Hou, M. (2020). A deep residual compensation extreme learning machine and applications. *Journal of Forecasting*, 39(6), 986-999. [CrossRef]

[13] Chen, Y., Yi, C., Xie, X., Hou, M., & Cheng, Y. (2020). Solution of ruin probability for continuous time model based on block trigonometric exponential neural network. *Symmetry*, 12(6), 876.[CrossRef]

[14] Saback, R. M., Conceicao, A. G. S., Santos, T. L. M., Albiez, J., & Reis, M. (2019). Nonlinear model predictive control applied to an autonomous underwater vehicle. *IEEE Journal of Oceanic Engineering*, 45(3), 799-812.[CrossRef]

[15] Zhang, B., Sun, X., Liu, S., & Deng, X. (2020). Adaptive model predictive control with extended state observer for multi-UAV formation flight. *International Journal of Adaptive Control and Signal Processing*, 34(10), 1341-1358. [CrossRef]

[16] Song, X., Shao, Y., & Qu, Z. (2019). A vehicle trajectory tracking method with a time-varying model based on the model predictive control. *IEEE Access*, 8, 16573-16583. [CrossRef]

[17] Wu, H., Si, Z., & Li, Z. (2020). Trajectory tracking control for four-wheel independent drive intelligent vehicle based on model predictive control. *IEEE Access*, 8, 73071-73081. [CrossRef]

[18] Li, S., Li, Z., Yu, Z., Zhang, B., & Zhang, N. (2019). Dynamic trajectory planning and tracking for autonomous vehicle with obstacle avoidance based on model predictive control. *IEEE Access*, 7, 132074-132086. [CrossRef]

[19] Al-Mayyahi, A., Aldair, A. A., & Rashid, A. T. (2020). Intelligent control of mobile robot via waypoints using nonlinear model predictive controller and quadratic bezier curves algorithm. *Journal of Electrical Engineering & Technology*, 15(4), 1857-1870. [CrossRef]

[20] Kim, E., Kim, J., & Sunwoo, M. (2014). Model predictive control strategy for smooth path tracking of autonomous vehicles with steering actuator dynamics. *International Journal of Automotive Technology*, 15, 1155-1164. [CrossRef]

[21] Britzelmeier, A., & Gerdts, M. (2020). A nonsmooth newton method for linear model-predictive control in tracking tasks for a mobile robot with obstacle avoidance. *IEEE Control Systems Letters*, 4(4), 886-891. [CrossRef]

[22] Yao, Z., Zhao, B., Yuan, T., Jiang, H., & Jiang, Y. (2020). Reducing gasoline consumption in mixed connected automated vehicles environment: A joint optimization framework for traffic signals and vehicle trajectory. *Journal of cleaner production*, 265, 121836. [CrossRef]

[23] Yang, X., Seethaler, R., Zhan, C., Lu, D., & Zhao, W. (2019). A model predictive contouring error precompensation method. *IEEE Transactions on Industrial Electronics*, 67(5), 4036-4045. [CrossRef]

[24] Hide, C., Moore, T., & Smith, M. (2004, April). Adaptive Kalman filtering algorithms for integrating GPS and low cost INS. In *Plans 2004. Position location and navigation symposium (ieee cat. no. 04ch37556)* (pp. 227-233). IEEE. [CrossRef]

[25] Bai, G., Liu, L., Meng, Y., Luo, W., Gu, Q., & Wang, J. (2019). Path tracking of wheeled mobile robots based on dynamic prediction model. *IEEE Access*, 7, 39690-39701. [CrossRef]

[26] Bai, G., Meng, Y., Liu, L., Luo, W., Gu, Q., & Li, K. (2019). A new path tracking method based on multilayer model predictive control. *Applied sciences*, 9(13), 2649. [CrossRef]

[27] Hang, P., Huang, S., Chen, X., & Tan, K. K. (2021). Path planning of collision avoidance for unmanned ground vehicles: A nonlinear model predictive control approach. Proceedings of the Institution of Mechanical Engineers, Part I: *Journal of Systems and Control Engineering*, 235(2), 222-236. [CrossRef]

[28] Gia Luan, P., & Thinh, N. T. (2020). Real-time hybrid navigation system-based path planning and obstacle avoidance for mobile robots. *Applied sciences*, 10(10), 3355. [CrossRef]

[29] C. Hong, Model Predictive control, Science Publishing House, Beijing, 2013.

[30] Yan, Z., Gong, P., Zhang, W., & Wu, W. (2020). Model predictive control of autonomous underwater vehicles for trajectory tracking with external disturbances. *Ocean Engineering*, 217, 107884. [CrossRef]

[31] Howard, S., Ko, H. L., & Alexander, W. E. (1996, March). Parallel processing and stability analysis of the Kalman filter. In *Conference Proceedings of the 1996 IEEE Fifteenth Annual International Phoenix Conference on Computers and Communications* (pp. 366-372). IEEE. [CrossRef]

[32] Oyelere, S. S. (2014). The application of model predictive control (MPC) to fast systems such as autonomous ground vehicles (AGV). *IOSR Journal of Computer Engineering*, 3(3), 27-37.

[33] Ephraim, Y., & Merhav, N. (2002). Hidden markov processes. *IEEE Transactions on information theory*, 48(6), 1518-1569. [CrossRef]

Hongyun Wu was born in Hubei, China, in 1976. He is the director of the Institute of Marine Mining at the Changsha Institute of Mining Research, holds a PhD in mechanical engineering, and is a senior engineer. His main research focus is on resource exploitation technology within the national long-term development project "International Regional Resource Development and Research." For over a decade, he has been dedicated to deep-sea resource development research. He has led or contributed as a key technical expert to more than ten projects, including the "Key Technology Research of 4-Wheel Drive Self-Propelled Mining Vehicle for 6,000-Meter Class Thin and Soft Substrate Mining Vehicle" and the "Development of Seabed Mineral Collection and Navigation and Positioning System." He has authored over 20 scientific research papers, with more than 10 indexed by EI.

Yuheng Chen was born in Suzhou, Jiangsu, China, in 1996. He holds an M.S. degree and is currently an assistant researcher in the School of Mechanical and Transportation at Hunan University. He also serves as the assistant director of the Key Laboratory of Advanced Design and Manufacturing for Vehicle Body at the College of Mechanical and Vehicle Engineering, Hunan University.

Hongmao Qin holds a Ph.D. and is a research professor in the School of Mechanical and Transportation at Hunan University. He is also the assistant director of the Key Laboratory of Advanced Design and Manufacturing for Vehicle Body at the College of Mechanical and Vehicle Engineering, Hunan University, and the assistant director of the Hunan Province Intelligent Transportation System Innovation Center. His research focuses on the safety system architecture design of intelligent transportation systems, specifically including functional safety, information security, and expected functional safety key technologies for intelligent driving systems, intelligent dispatching systems, and intelligent interconnection systems. He has contributed significantly to the industrialization of intelligent mining systems, intelligent marine systems, and intelligent express transportation systems, achieving notable innovative progress.

In recent years, he has published over 30 academic papers, including 19 indexed by SCI/EI. He has applied for or been granted 15 invention patents and 4 computer software copyrights. He has led or participated in more than 10 key projects, including those funded by the National Natural Science Foundation of China, the 863 Program, and Science and Technology Support initiatives. Additionally, he has undertaken 4 national/industry/group standards, resulting in substantial economic and social benefits.